

POWERFUL LOSSY COMPRESSION FOR NOISY IMAGES

Shilv Cai^{1,2}, Xiaoguo Liang^{1,2}, Shuning Cao^{1,2}, Luxin Yan^{1,2}, Sheng Zhong^{1,2}, Liqun Chen^{1,2,†}, Xu Zou^{1,2}

¹ Huazhong University of Science and Technology, China

² National Key Laboratory of Multispectral Information Intelligent Processing Technology, China
{caishilv, liangxiaoguo, sn_cao, yanluxin, zhongsheng, chenliqun, zoux}@hust.edu.cn

ABSTRACT

Image compression and denoising represent fundamental challenges in image processing with many real-world applications. To address practical demands, current solutions can be categorized into two main strategies: 1) sequential method; and 2) joint method. However, sequential methods have the disadvantage of error accumulation as there is information loss between multiple individual models. Recently, the academic community began to make some attempts to tackle this problem through end-to-end joint methods. Most of them ignore that different regions of noisy images have different characteristics. To solve these problems, in this paper, our proposed signal-to-noise ratio (SNR) aware joint solution exploits local and non-local features for image compression and denoising simultaneously. We design an end-to-end trainable network, which includes the main encoder branch, the guidance branch, and the signal-to-noise ratio (SNR) aware branch. We conducted extensive experiments on both synthetic and real-world datasets, demonstrating that our joint solution outperforms existing state-of-the-art methods.

Index Terms— Joint Solution, Image Compression, Image Denoising, Neural Networks

1. INTRODUCTION

Image denoising, a vital task in low-level computer vision, plays a crucial role in numerous high-level applications. The recent years have marked remarkable advancements in image denoising, primarily attributed to the adoption of sophisticated deep neural networks. In real-world scenarios, lossy image compression is essential for efficient media storage and transmission. In recent years, learning-based lossy image compression methods [1][2][3] have made significant progress, outperforming traditional standards on performance metrics such as peak signal-to-noise ratio (PSNR) and multi-scale structural similarity index (MS-SSIM). Given that the majority of current compression approaches are tailored for general images. These compressors perceive noise as essential information and allocate bits explicitly to preserve it, disregarding the fact that noise is typically undesired by ordinary

users, abbreviated as “bits misallocation problem”. As mentioned in previous research [4][5], image noise can degrade image compression quality.

In various real-world systems such as autonomous driving and visual surveillance, there is a requirement for lossy noisy image compression, while minimal research has been conducted in the academic community regarding this practical subject. Existing engineering solutions can be classified into two manners: “Compress before Denoise” and “Denoise before Compress”. However, those sequential solutions have the disadvantage of error accumulation as there is information loss between multiple individual models. More specifically, the “Compress before Denoise” solution tends to suffer from bits misallocation. In the case of the “Denoise before Compress” solution, the rate-distortion performance of the compression method is predominantly constrained by the denoising approach. The quality of the denoised image will be further degraded after using the lossy codec.

In addition to the aforementioned sequential solutions, the academic community has recently made some attempts to tackle this problem through end-to-end joint manners [6][7][8]. Most of them ignore that the different regions in the noisy image have different characteristics. In this paper, we present a key insight that different regions within a noisy image may exhibit distinct characteristics. More specifically, regions with complex textures are significantly impacted by noise, whereas areas with fewer textures in the same image may experience only mild interference. To achieve superior reconstruction results, it is crucial to adaptively consider the distinct characteristics of various regions within the noisy images during the encoding and denoising procedure.

To achieve spatially varying image denoising and compression simultaneously, we investigate the relationship between signal and noise in image space through the exploration of signal-to-noise ratio (SNR) [9]. Regions with lower SNR often exhibit unclear details and substantial noise interference. To address this, we leverage non-local image information across a long spatial range for effective image denoising and compression. Conversely, regions with relatively higher SNR experience fewer noise interferences, making local image information generally adequate. Based on these considerations, in this work, our proposed joint solution is to collec-

[†]Corresponding Author.

tively exploit local and non-local information for image compression and denoising. We formulate an end-to-end trainable architecture with three branches: 1) the main encoder branch extracts compressed domain features, 2) the teacher guidance branch generates two-level guiding features, 3) the signal-to-noise ratio (SNR) aware branch captures local and non-local features. The local/non-local features are fused with the compressed domain features, producing denoised features that enable simultaneous image compression and denoising. Finally, denoised images are reconstructed through the main decoder. In summary, the contributions of this work are as follows:

- We propose a new signal-to-noise (SNR) aware framework that extracts local and non-local features for joint image compression and denoising with the SNR prior.
- The end-to-end trainable three-branch architecture empowers the joint solution to obtain high-quality reconstructed images at low bits-per-pixel (BPP).
- We conduct extensive experiments on both synthetic and real-world datasets, demonstrating that our proposed SNR-aware joint framework consistently outperforms state-of-the-art methods.

2. RELATED WORKS

2.1. Learning-based Lossy Image Compression

The works [10][11][12] initially used neural networks for end-to-end image compression and inspired many subsequent learning-based image compression methods. Subsequent researchers have conducted extensive research on the three components typically involved in lossy image compression: transformation, quantization, and entropy coding. Some previous research focuses on quantization, *e.g.*, Dumas *et al.* [13] aimed to learn different quantization step sizes for various latent representations. Some works focus on the transform, *e.g.*, residual block [12], attention module [14], and transformer-based architecture [2]. Some works aim to improve the efficiency of entropy coding, *e.g.*, channel-wise entropy model [15], checkerboard context model [1], and multivariate Gaussian mixture model [3]. However, the mutual influence with image processing tasks is not considered in the design of most existing learning-based compression methods. Combined with image processing tasks in the practical systems, this can lead to unsatisfactory image quality and suboptimal subsequent visual tasks.

2.2. Image Denoising

Image denoising is an image restoration task that has been studied for a long time, and many traditional methods have been proposed in the past decades. Those traditional methods [16][17][18] are typically designed by exploiting certain signal structures or noise characteristics that do not rely on

data-driven learning. As neural networks are rapidly developing, more and more methods are utilizing neural networks to improve image-denoising performance. There have been some works on adapting synthetic dataset approaches to real-world scenarios [19][20]. Recently, the performance has been further improved by some state-of-the-art methods [21][22]. However, many learning-based methods are designed without considering the effects on other tasks (*e.g.*, image compression). This is suboptimal in the real-world image processing pipeline which typically involves multiple tasks, such as image denoising and image compression.

2.3. Joint Solutions

Some joint solutions [23][24] have been verified as an effective alternative to sequential ones with promising results in the image processing pipeline. Testolina *et al.* [6] introduced the idea of denoising into image decompression by denoising the latent representations during the decoding procedure. Cheng *et al.* [7] designed a plug-in module that can perform denoising during image encoding processing. Alvar *et al.* [25] used scalable coding to divide the bitstream into useful image information and noise. Huang *et al.* [8] proposed the Noise-Adaptive ResNet VAE (NARV) to handle both clean and noisy images by a single image compression model. However, the above-mentioned methods of joint image compression and image denoising ignored that the different regions in the noisy image have different characteristics. These characteristics can be utilized to efficiently identify useful content and noise in the image, allowing for higher image compression and image denoising performance.

3. PROPOSED METHOD

3.1. Framework

Overall workflow. Fig. 1 depicts the overview of the network architecture of our proposed signal-to-noise ratio (SNR) aware joint image compression and denoising framework. The joint framework contains a novel three-branch design for the training procedure. The noisy image \tilde{x} is transformed to the denoised compressed domain latent representation y through the main encoder g_{a0} and g_{a1} with the signal-to-noise ratio (SNR) aware branch. Then, quantization of y to the discrete denoised compressed domain latent representation \hat{y} is performed by the quantizer Q . During the training procedure, we replace the non-differentiable quantization operation with the addition of uniform noise $U(-\frac{1}{2}, \frac{1}{2})$ to the denoised compressed domain latent representation y . During the testing procedure, we round the denoised compressed domain latent representation y , directly. The hyper-prior scale entropy model [14][26] is utilized in our proposed framework to effectively estimate the distribution $p_{\hat{y}|\tilde{z}} \sim \mathcal{N}(\mu, \sigma^2)$ of the discrete denoised compressed latent representation \hat{y} . The Gaussian parameters μ and σ are generated by the entropy model to

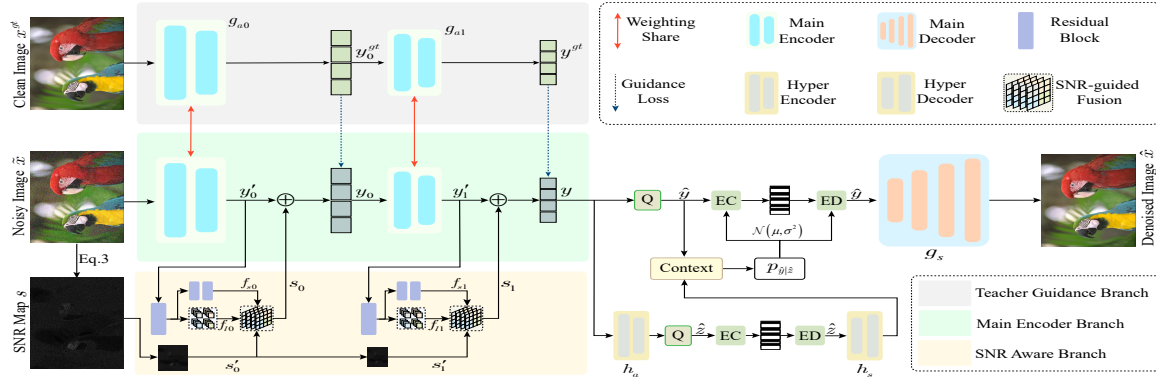


Fig. 1: The network architecture of proposed SNR-aware joint solution of image compression and denoising. The architecture contains three branches, “Teacher Guidance Branch”, “Main Encoder Branch” and “SNR Aware Branch”, in the left half of the figure. The right half of the figure contains the main decoder, entropy models, context model, and hyper encoder/decoder commonly used in recent learning-based compression method [14]. Note that the “Teacher Guidance Branch” is for training only, the “Main Encoder Branch” and “SNR Aware Branch” are activated during training of the entire network and used for inference. \oplus denotes the addition by element.

support the entropy encoding/decoding procedure. The range asymmetric numeral system [27] is used to losslessly encode discrete denoised features \hat{y} and latent representation z into bitstreams. The latent representation z is quantized using the same strategy as the denoised compressed latent representation y . The factorized entropy model [10] is used to estimate the distribution p_z of the discrete latent representation \hat{z} . The entropy decoding yields the discrete denoised compressed latent representation \hat{y} , which is then fed into the main decoder g_s to reconstruct the denoised image \hat{x} .

Three branch architecture. As shown in Fig. 1, our proposed joint solution consists of three branches: 1) the main encoder branch, 2) the teacher guidance branch, and 3) the signal-to-noise ratio (SNR) aware branch. During the training procedure, the noisy image \tilde{x} and the corresponding clean image x^{gt} are fed into three branches, respectively. The main encoder branch combines the compressed domain features (y_0'/y_1') with the local/non-local information (s_0 and s_1) generated by the SNR-aware branch to obtain the denoised compressed domain latent representation (y_0/y_1); the calculation process is abbreviated as: $SNR(\cdot, \cdot)$. The SNR aware branch generates local/non-local features (s_0/s_1) through SNR map s . The SNR map s is achieved through a simple yet effective non-learning-based denoising operation (refer Eq.3). In addition, the clean image x^{gt} is fed to the teacher guidance branch (training procedure only) to generate two-level guiding features (y_0^{gt}/y_1^{gt}) by the main encoder blocks (g_{a0}/g_{a1}), respectively. The two-level guidance and denoised compressed latent representation y_0^{gt}/y_1^{gt} and y_0/y_1 can be expressed by formulas:

$$\begin{aligned} y_0^{gt} &= g_{a0}(x^{gt}), & y_0 &= g_{a0}(\tilde{x}) + SNR(s_0, g_{a0}(\tilde{x})), \\ y_1^{gt} &= g_{a1}(y_0^{gt}), & y &= g_{a1}(y_0) + SNR(s_1, g_{a1}(y_0)). \end{aligned} \quad (1)$$

During the training procedure, the L_1 distance between denoised and guidance latent representation is minimized:

$$\mathcal{L}_g = \|y_0^{gt} - y_0\|_1 + \|y_1^{gt} - y_1\|_1. \quad (2)$$

3.2. SNR-Aware Denoising in Compressed Features

The signal-to-noise ratio (SNR) map $s \in \mathbb{R}^{h \times w}$ is obtained by converting the noisy image $\tilde{x} \in \mathbb{R}^{3 \times h \times w}$ to the grayscale image $\hat{x} \in \mathbb{R}^{h \times w}$ and then using the following formulas:

$$\hat{x} = kernel(\tilde{x}), \quad n = abs(\hat{x} - \tilde{x}), \quad s = \frac{\hat{x}}{n}, \quad (3)$$

where $kernel(\cdot)$ represents the operation of averaging local pixel groups, while $abs(\cdot)$ indicates the application of the absolute value function. As shown in Fig. 1, we utilize the “Residual Block” to extract features. These features are subsequently processed separately by the long- and short-range modules, resulting in the generation of non-local features (f_{l0}/f_{l1}) and local features (f_{s0}/f_{s1}). The two-level local and non-local features are fused. It is illustrated in “SNR-guided Fusion” of Fig. 1 and is calculated as follows:

$$\begin{aligned} s_0 &= f_{s0} \times s'_0 + f_{l0} \times (1 - s'_0), \\ s_1 &= f_{s1} \times s'_1 + f_{l1} \times (1 - s'_1), \end{aligned} \quad (4)$$

where s'_0 and s'_1 are resized from SNR map s according to the shape of local/non-local features ($f_{s0}/f_{s1}/f_{l0}/f_{l1}$). The SNR-aware fusion features, represented as s_0/s_1 , are added to the main features (y_0'/y_1') to generate the denoised compressed latent representation (y_0/y_1).

Short-range modules are constructed using a few residual blocks. Long-range modules are constructed by SNR-aware transformers with self-attention blocks. In the long-range modules, the feature maps $F \in \mathbb{R}^{h \times w \times C}$ are divided into t feature patches, represented as $F^i \in \mathbb{R}^{m \times m \times C}$,

$i = \{1, \dots, t\}$. The relationship between patch size $m \times m$ and the entire feature map can be described as $t = \frac{h}{m} \times \frac{w}{m}$. The feature patches F^1, \dots, F^t is flattened into 1D vectors, and processed by:

$$\begin{aligned} f^0 &= [F^1, F^2, \dots, F^t], \\ q^i &= k^i = v^i = LN(f^{i-1}), \\ \hat{f}^i &= MSA(q^i, k^i, v^i) + f^{i-1}, \\ f^i &= FFN(LN(\hat{f}^i)) + \hat{f}^i, \\ [\tilde{\mathcal{F}}^1, \tilde{\mathcal{F}}^2, \dots, \tilde{\mathcal{F}}^t] &= f^r, i \in \{1, 2, \dots, r\}. \end{aligned} \quad (5)$$

Where $LN(\cdot)$ is layer normalization. f^i is the result calculated by i -th transformer block. $MSA(\cdot)$ is the multi-head self-attention module [28]. $FFN(\cdot)$ is the feed-forward network [28]. $q^i, k^i,$ and v^i represent query, key, and value vectors, respectively. r is the number of layers in the transformer. $\tilde{\mathcal{F}}^1, \tilde{\mathcal{F}}^2, \dots, \tilde{\mathcal{F}}^t$ are the outputs of the transformer block which can be reshaped into 2D feature map (f_{i0}/f_{i1}).

3.3. Rate-Distortion Optimization

In terms of image compression, we aim to minimize the length of the stored bitstreams; while for image denoising, we aim to minimize the difference between the decoded image \hat{x} and the paired clean image x^{gt} . Thus in this joint task, we can use the rate-distortion (RD) objective function as follows:

$$\mathcal{L}_{rd} = \mathfrak{R}(\hat{y}) + \mathfrak{R}(\hat{z}) + \lambda_d \cdot \mathfrak{D}(\hat{x}, x^{gt}), \quad (6)$$

where the $\mathfrak{D}(\hat{x}, x^{gt})$ is the distortion between decoded denoising image \hat{x} and clean image x^{gt} . Similar to previous works [11][14], the $\mathfrak{R}(\cdot)$ represents the compression level of the discrete latent representations \hat{y}, \hat{z} (as shown in Fig. 1), defined as follows:

$$\mathfrak{R}(\hat{y}) = \mathbb{E}_{q_{\hat{y}}}[-\log p_{\hat{y}|\hat{z}}(\hat{y}|\hat{z})], \mathfrak{R}(\hat{z}) = \mathbb{E}_{q_{\hat{z}}}[-\log p_{\hat{z}|\theta}(\hat{z}|\theta)]. \quad (7)$$

λ_d denotes the weighting coefficient, which is the trade-off between compression levels and distortion. Considering guidance loss Eq.2, the objective function of the entire network is:

$$\mathcal{L} = \mathcal{L}_{rd} + \lambda_g \cdot \mathcal{L}_g, \quad (8)$$

where the parameter $\lambda_g = 3$ represents the weight factor assigned to the guidance loss.

4. EXPERIMENTS

4.1. Datasets and Implementation details

Synthetic datasets. The training and validation dataset is Flickr 2W [29]. Images smaller than 256 pixels are excluded, and approximately 200 images are chosen for validation. During the training procedure, randomly cropped

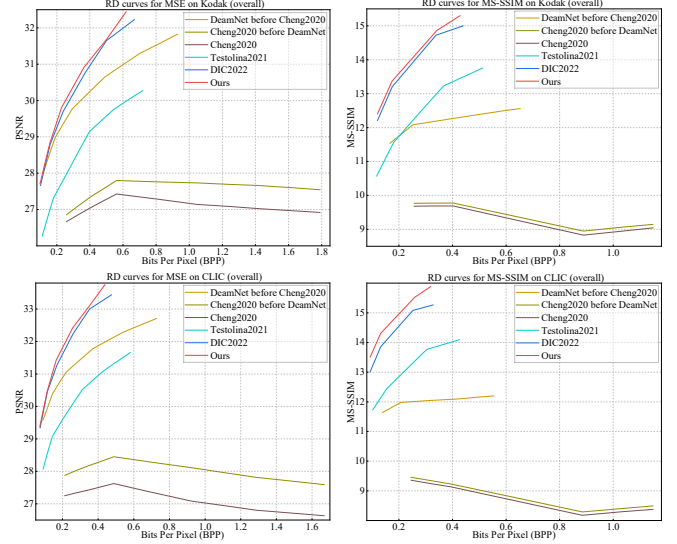


Fig. 2: Overall RD curves for the Kodak and CLIC datasets across all noise levels. Our proposed joint solution, indicated by red curves, exhibits superior RD performance compared to pure compression, sequential, and joint methods.

patches with a resolution of 256×256 pixels are used to optimize the joint framework. The CLIC [30] Professional Validation and Kodak [31] datasets are employed for testing. For more details about noise synthesis, please refer to the supplementary material.

Real-world datasets. The proposed joint framework is trained using the SIDD Medium [32] dataset, consisting of 320 pairs of noisy-clear sRGB images in the training set. Subsequently, real-world noisy images are utilized in the testing procedure. The models undergo validation using the 1280 patches from the SIDD validation set and are tested on the SIDD benchmark patches, with the results submitted for testing on the SIDD website.

Implementation details. Our implementation relies on PyTorch and the open-source CompressAI library. The networks are optimized using the Adam optimizer with a mini-batch size of 16, trained for approximately 600 epochs on RTX 3090 GPUs. The initial learning rate is set as 5×10^{-5} and decayed by a factor of 0.1 at epochs 450 and 500. We set a loss cap for each model, ensuring that the network skips optimizing a mini-step if the training loss exceeds the specified threshold. We train MSE models across 6 qualities, with λ_d selected from the set $\{0.0018, 0.0035, 0.0067, 0.0130, 0.0250, 0.0483\}$; the corresponding λ_d values for MS-SSIM models are chosen from $\{4.58, 8.73, 31.73, 60.50\}$. For improved visualization, the MS-SSIM is converted to decibels using the formula $-10 \log_{10}(1 - \text{MS-SSIM})$.

4.2. Rate-Distortion Performance

Our proposed joint solution compares with the five methods: 1) ‘‘DIC2022’’: the state-of-the-art joint method [7]; 2)

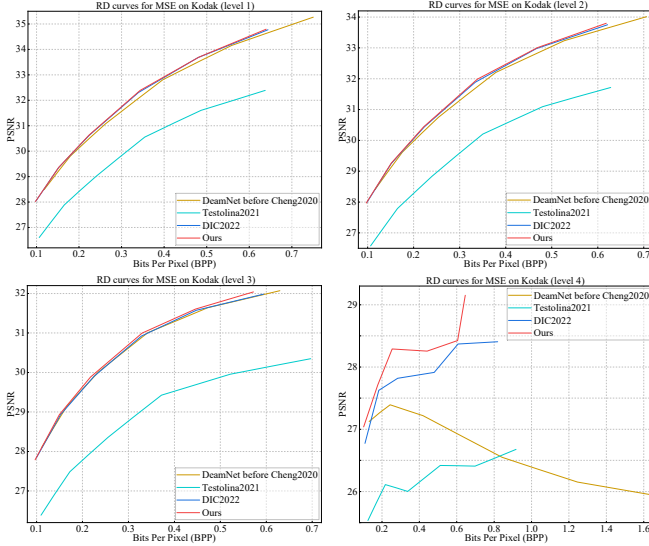


Fig. 3: RD curves on the Kodak dataset at various noise levels. Our method surpasses both sequential and joint methods, particularly at the high noise level. This denotes that the proposed SNR-aware branch efficiently captures valuable information through a combination of local and non-local features.

“Testolina2021”: an early joint method [6]; 3) “Cheng2020 before DeamNet”: sequential method of Cheng2020 [14] and DeamNet [33]; 4) “DeamNet before Cheng2020”: sequential method of DeamNet [33] and Cheng2020 [14]; 5) “Cheng2020”: the compression method [14] is used on noise-to-clean image pairs directly. RD results are obtained from the CompressAI evaluation platform, the official SIDD website, or provided in the corresponding paper. More experimental results, both quantitative and visual, are provided in the supplementary material.

Synthetic noise (overall). In Fig. 2, we present overall RD curves for both MSE and MS-SSIM methods, covering all four noise levels, as evaluated on the Kodak and CLIC datasets, respectively. Our proposed joint solution, depicted by the red RD curves, outperforms the pure compression, sequential, and joint methods in terms of overall performance.

Synthetic noise (individual). To delve deeper into the impact of various noise levels, Fig. 3 illustrates RD curves for MSE models on the Kodak dataset at individual noise levels. Our proposed joint method is better than the sequential and joint methods, especially at the high noise level. The SNR in an image is usually low when the noise level is high. Therefore, it is difficult to achieve high-quality reconstructed images using only local features. Thanks to our proposed SNR-aware branch through local and non-local feature fusion, we can effectively be aware of different SNR regions in the image and then obtain a higher-quality reconstructed image. More experimental results are provided in the supplementary material.

Real-world noise. In Fig. 4, we present the RD curves optimized for MSE on the SIDD test set with real-world noise.

The purple dashed line indicates the results of the pure denoising model DeamNet [33] to show the upper bound of the denoising performance without compression (BPP = 24). The results demonstrate the effectiveness of our proposed joint framework, proving its efficiency not only on synthetic datasets but also on images containing real-world noise.

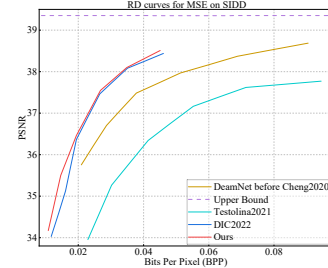


Fig. 4: RD performance curves optimized by MSE aggregated on SIDD. Our proposed method achieved the best RD performance. This indicates that our method is robust on real noisy images. The purple dotted line serves as a reference for the DeamNet [33] ideal case without compression.

5. CONCLUSION

We introduce an innovative signal-to-noise ratio (SNR) aware joint solution to improve the capability of lossy image compression for noisy images. Thanks to the end-to-end trainable three-branch architecture, the joint solution can achieve high-quality denoised images at low BPP. The different regions in the noisy image have different characteristics, these characteristics can be utilized in the local and non-local information fusion procedure efficiently. Local and non-local information obtained by the SNR-aware branch would be fused with the compressed features to generate compressed denoised features. Finally, the denoised image can be obtained by decoding the compressed denoised features directly. The experimental results show that our proposed SNR-aware joint solution surpasses sequential and joint methods on both synthetic and real-world datasets.

6. ACKNOWLEDGMENTS

This work was supported by the National Natural Science Foundation of China under Grant 62301228, 62176100. The computation is completed in the HPC Platform of Huazhong University of Science and Technology.

7. REFERENCES

- [1] Dailan He, Yaoyan Zheng, Baocheng Sun, Yan Wang, and Hongwei Qin, “Checkerboard context model for efficient learned image compression,” in *CVPR*, 2021.
- [2] Yichen Qian, Ming Lin, Xiuyu Sun, Zhiyu Tan, and Rong Jin, “Entroformer: A transformer-based entropy model for learned image compression,” in *ICLR*, 2022.

- [3] Xiaosu Zhu, Jingkuan Song, Lianli Gao, Feng Zheng, and Heng Tao Shen, “Unified multivariate gaussian mixture for efficient neural image compression,” in *CVPR*, 2022.
- [4] Osama K Al-Shaykh and Russell M Mersereau, “Lossy compression of noisy images,” *TIP*, vol. 7, no. 12, pp. 1641–1652, 1998.
- [5] Nikolay Ponomarenko, Sergey Krivenko, Vladimir Lukin, Karen Egiazarian, and Jaakko T Astola, “Lossy compression of noisy images based on visual quality: a comprehensive study,” *EURASIP Journal on Advances in Signal Processing*, vol. 2010, pp. 1–13, 2010.
- [6] Michela Testolina, Evgeniy Upenik, and Touradj Ebrahimi, “Towards image denoising in the latent space of learning-based compression,” in *Applications of Digital Image Processing XLIV*, 2021.
- [7] Ka Leong Cheng, Yueqi Xie, and Qifeng Chen, “Optimizing image compression via joint learning with denoising,” in *ECCV*, 2022.
- [8] Yuning Huang, Zhihao Duan, and Fengqing Zhu, “Narv: An efficient noise-adaptive resnet vae for joint image compression and denoising,” in *ICMEW*, 2023.
- [9] Damon M Chandler and Sheila S Hemami, “Vsnr: A wavelet-based visual signal-to-noise ratio for natural images,” *TIP*, vol. 16, no. 9, pp. 2284–2298, 2007.
- [10] Johannes Ballé, Valero Laparra, and Eero P Simoncelli, “End-to-end optimized image compression,” in *ICLR*, 2017.
- [11] Johannes Ballé, David Minnen, Saurabh Singh, Sung Jin Hwang, and Nick Johnston, “Variational image compression with a scale hyperprior,” in *ICLR*, 2018.
- [12] Lucas Theis, Wenzhe Shi, Andrew Cunningham, and Ferenc Huszár, “Lossy image compression with compressive autoencoders,” *ICLR*, 2017.
- [13] Thierry Dumas, Aline Roumy, and Christine Guillemot, “Autoencoder based image compression: Can the learning be quantization independent?,” in *ICASSP*, 2018.
- [14] Zhengxue Cheng, Heming Sun, Masaru Takeuchi, and Jiro Katto, “Learned image compression with discretized gaussian mixture likelihoods and attention modules,” in *CVPR*, 2020.
- [15] David Minnen and Saurabh Singh, “Channel-wise autoregressive entropy models for learned image compression,” in *ICIP*, 2020.
- [16] Antonin Chambolle, “An algorithm for total variation minimization and applications,” *Journal of Mathematical imaging and vision*, vol. 20, pp. 89–97, 2004.
- [17] Antoni Buades, Bartomeu Coll, and J-M Morel, “A non-local algorithm for image denoising,” in *CVPR*, 2005.
- [18] Shuhang Gu, Lei Zhang, Wangmeng Zuo, and Xiangchu Feng, “Weighted nuclear norm minimization with application to image denoising,” in *CVPR*, 2014.
- [19] Shi Guo, Zifei Yan, Kai Zhang, Wangmeng Zuo, and Lei Zhang, “Toward convolutional blind denoising of real photographs,” in *CVPR*, 2019.
- [20] Yoonsik Kim, Jae Woong Soh, Gu Yong Park, and Nam Ik Cho, “Transfer learning from synthetic to real-noise denoising with adaptive instance normalization,” in *CVPR*, 2020.
- [21] Zutao Jiang, Changlin Li, Xiaojun Chang, Ling Chen, Jihua Zhu, and Yi Yang, “Dynamic slimmable denoising network,” *TIP*, vol. 32, pp. 1583–1598, 2023.
- [22] Haoyu Chen, Jinjin Gu, Yihao Liu, Salma Abdel Magid, Chao Dong, Qiong Wang, Hanspeter Pfister, and Lei Zhu, “Masked image training for generalizable deep image denoising,” in *CVPR*, 2023.
- [23] Thibaud Ehret, Axel Davy, Pablo Arias, and Gabriele Facciolo, “Joint demosaicking and denoising by fine-tuning of bursts of raw images,” in *ICCV*, 2019.
- [24] Wenzhu Xing and Karen Egiazarian, “End-to-end learning for joint image demosaicing, denoising and super-resolution,” in *CVPR*, 2021.
- [25] Saeed Ranjbar Alvar, Mateen Ulhaq, Hyomin Choi, and Ivan V Bajić, “Joint image compression and denoising via latent-space scalability,” *Frontiers in Signal Processing*, vol. 2, pp. 932873, 2022.
- [26] David Minnen, Johannes Ballé, and George D Toderici, “Joint autoregressive and hierarchical priors for learned image compression,” in *NeurIPS*, 2018.
- [27] Jarek Duda, “Asymmetric numeral systems: Entropy coding combining speed of huffman coding with compression rate of arithmetic coding,” *arXiv preprint arXiv:1311.2540*, 2013.
- [28] Ashish Vaswani, Noam Shazeer, Niki Parmar, Jakob Uszkoreit, Llion Jones, Aidan N Gomez, Lukasz Kaiser, and Illia Polosukhin, “Attention is all you need,” in *NeurIPS*, 2017.
- [29] Jiaheng Liu, Guo Lu, Zhihao Hu, and Dong Xu, “A unified end-to-end framework for efficient deep image compression,” *arXiv preprint arXiv:2002.03370*, 2020.
- [30] George Toderici, Wenzhe Shi, Radu Timofte, Johannes Balle Lucas Theis, Eirikur Agustsson, Nick Johnston, and Fabian Mentzer, “Workshop and challenge on learned image compression,” 2021.
- [31] Eastman Kodak Company, “Kodak lossless true color image suite,” 1999.
- [32] Abdelrahman Abdelhamed, Stephen Lin, and Michael S Brown, “A high-quality denoising dataset for smartphone cameras,” in *CVPR*, 2018.
- [33] Chao Ren, Xiaohai He, Chuncheng Wang, and Zhibo Zhao, “Adaptive consistency prior based deep network for image denoising,” in *CVPR*, 2021.
- [34] Ben Mildenhall, Jonathan T Barron, Jiawen Chen, Dillon Sharlet, Ren Ng, and Robert Carroll, “Burst denoising with kernel prediction networks,” in *CVPR*, 2018.
- [35] Adam Paszke, Sam Gross, Francisco Massa, Adam Lerer, James Bradbury, Gregory Chanan, Trevor

Killeen, Zeming Lin, Natalia Gimelshein, Luca Antiga, Alban Desmaison, Andreas Kopf, Edward Yang, Zachary DeVito, Martin Raison, Alykhan Tejani, Sasank Chilamkurthy, Benoit Steiner, Lu Fang, Junjie Bai, and Soumith Chintala, “Pytorch: An imperative style, high-performance deep learning library,” in *NeurIPS*, 2019.

- [36] Jean Bégaint, Fabien Racapé, Simon Feltman, and Akshay Pushparaja, “Compressai: a pytorch library and evaluation platform for end-to-end compression research,” *arXiv preprint arXiv:2011.03029*, 2020.
- [37] Diederik P. Kingma and Jimmy Ba, “Adam: A method for stochastic optimization,” in *ICLR*, 2015.
- [38] Yueqi Xie, Ka Leong Cheng, and Qifeng Chen, “Enhanced invertible encoding for learned image compression,” in *ACM MM*, 2021.
- [39] Joint Video Experts Team (JVET), “Vvc official test model vtm,” Accessed on April 5, 2021.
- [40] Fabrice Bellard, “Bpg image format,” 2015.

Summary

This supplementary material is organized as follows:

- Section A describes more details about noise synthesis.
- Section B provides more RD performance comparison results on the CLIC Professional Validation [30] dataset.
- Section C shows our proposed method is used for general image compression. It indicates our framework is also effective for compressing generic images.
- Section D provides visualization results.

A. NOISE SYNTHESIS

We use the same noise synthesis strategy as prior research [34]. In the training procedure, we acquire the noise parameter δ_r and shot noise parameter δ_s through uniform sampling from the intervals $[10^{-3}, 10^{-1.5}]$ and $[10^{-4}, 10^{-2}]$, respectively. During testing and validation procedures, we utilize the four pre-determined parameter pairs $\{\text{Gain} \propto 1 = (10^{-2.1}, 10^{-2.6}), \text{Gain} \propto 2 = (10^{-1.8}, 10^{-2.3}), \text{Gain} \propto 4 = (10^{-1.4}, 10^{-1.9}), \text{Gain} \propto 8 = (10^{-1.1}, 10^{-1.5})\}$. It is worth noting that, the network is unaware of the $\text{Gain} \propto 4 = (10^{-1.4}, 10^{-1.9})$ (slightly noisier) and $\text{Gain} \propto 8 = (10^{-1.1}, 10^{-1.5})$ (significantly noisier) levels. We test the Kodak and CLIC Professional Validation datasets at full resolution with predetermined noise levels.

B. MORE EXPERIMENTAL RESULTS

Fig. 5 illustrates RD curves for MSE models on the CLIC dataset at individual noise levels to delve deeper into the impact of various noise levels. Our proposed joint method is better than the state-of-the-art joint method, especially at the high noise level. The signal-to-noise ratio (SNR) in an image is usually low when the noise level is high. Therefore, it is difficult to achieve high-quality reconstructed images using only local features. With our proposed SNR-aware branch through local and non-local feature fusion, we can effectively be aware of different SNR regions in noisy images and obtain higher-quality reconstructed images.

C. COMPRESSING GENERIC IMAGES

We use the proposed network framework for compressing generic natural images. The training dataset is Flickr 2W [29]. We discard images with a resolution of less than 512×512 in the dataset preprocessing stage. Randomly cropped patches with a resolution of 512×512 pixels are used to optimize the network. Our implementation relies on Pytorch [35] and an open-source CompressAI PyTorch library [36]. The networks are optimized us-

ing the Adam [37] optimizer with a mini-batch size of 8 for approximately 2500000 iterations and trained on RTX 3090 GPUs. The initial learning rate is set as 10^{-4} and decayed by a factor of 0.5 at iterations 800000, 1000000, 1200000, 1400000, 1600000, and 1800000. We train our models under 6 qualities, where λ_d is selected from the set $\{0.0018, 0.0036, 0.0072, 0.013, 0.026, 0.0483\}$.

We evaluate the rate-distortion performance on Kodak [31] and CLIC Professional Validation [30] dataset. The rate-distortion performance comparison results of the proposed framework with the Cheng2020-anchor [14], ACM MM2021 [38], VTM [39] and BPG [40] are shown in Fig. 6. To achieve maximum compression performance, both VVC and BPG software are configured to utilize the YUV444 format. The SNR-aware branch effectively captures local and no-local information about the original images which is useful for improving the rate-distortion performance. As the experimental results show, our proposed framework is better than the baseline [14] in terms of rate-distortion performance, indicating that our proposed joint framework is also effective for compressing generic natural images.

D. QUALITATIVE RESULTS

To further demonstrate the effectiveness of our method, we provide qualitative comparisons with the state-of-the-art joint method DIC2022 [7]. Specifically, we show the visual results of the sample CLIC Professional Validation dataset [30] images at noise level 4 ($\text{Gain} \propto 8 = (10^{-1.1}, 10^{-1.5})$). These results show that our proposed SNR-aware joint method achieves superior reconstructed image quality even at lower bits per pixel (BPP). In other words, our proposed joint method effectively leverages its awareness of different signal-to-noise ratio (SNR) regions in the image, resulting in a significantly improved quality of the reconstructed image.

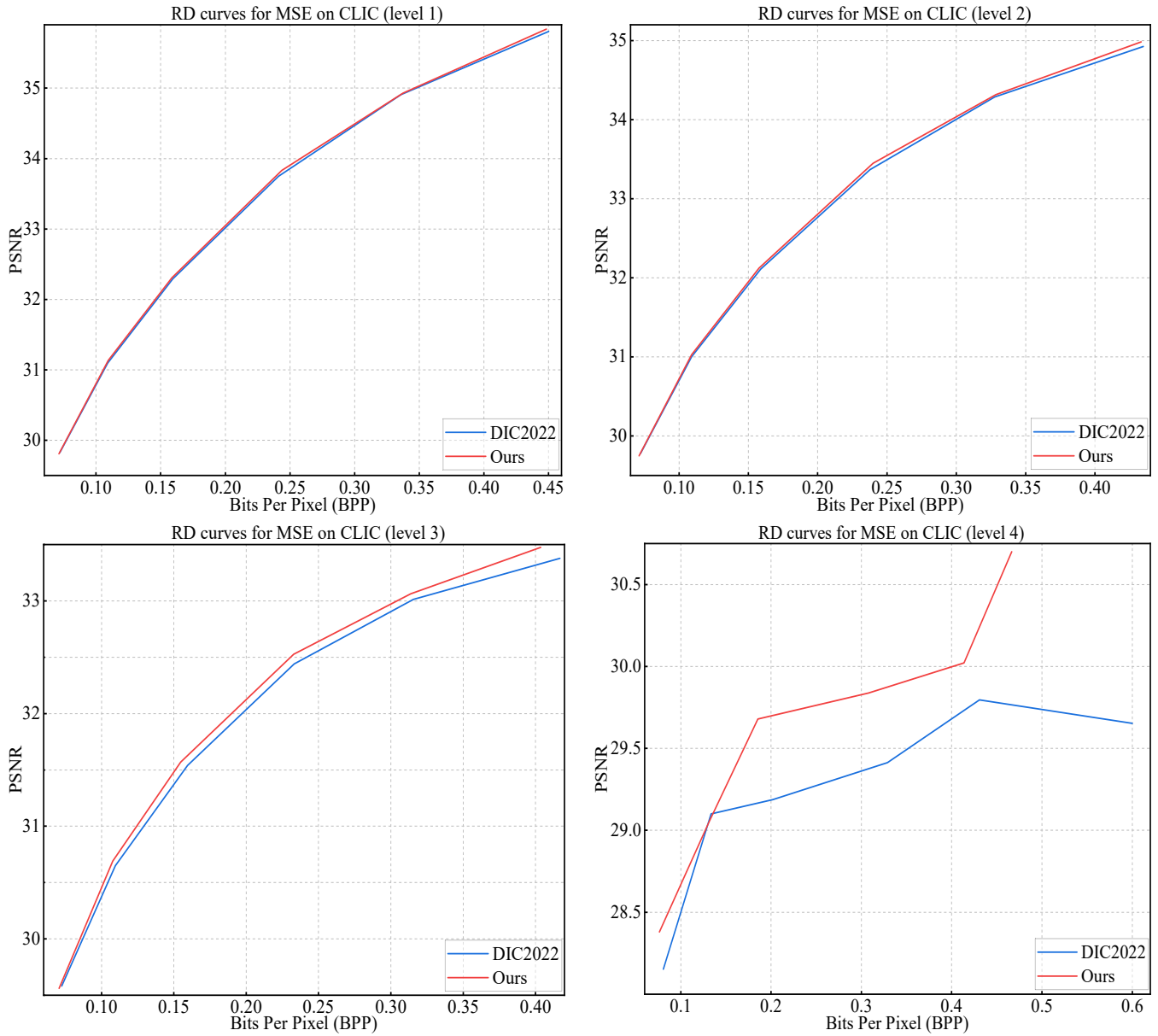
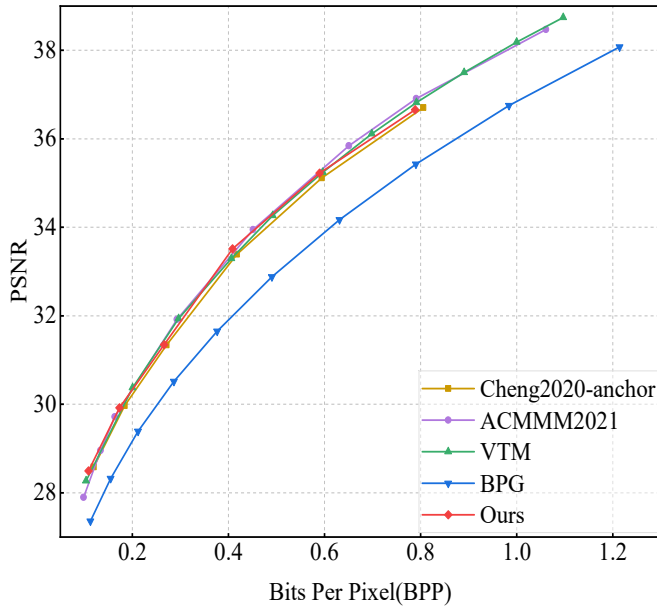
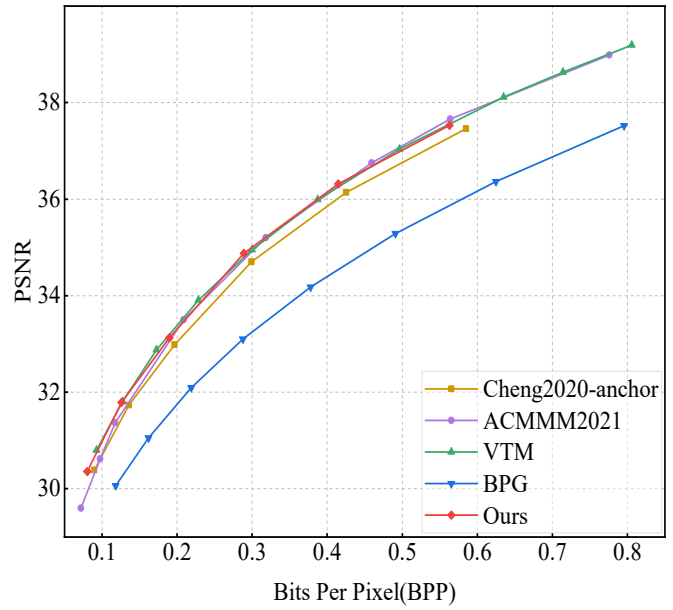


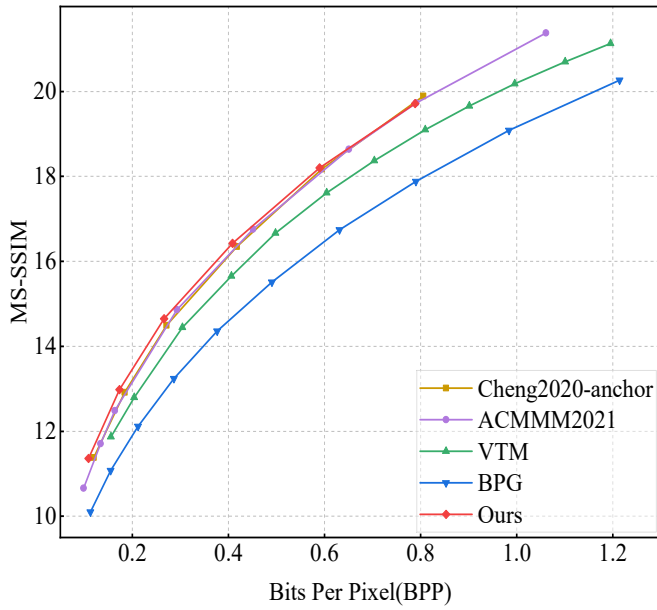
Fig. 5: RD curves on the CLIC dataset at various noise levels. Our method surpasses the state-of-the-art joint method, particularly at the high noise level. This denotes that the proposed SNR-aware branch efficiently captures valuable information through a combination of local and non-local features.



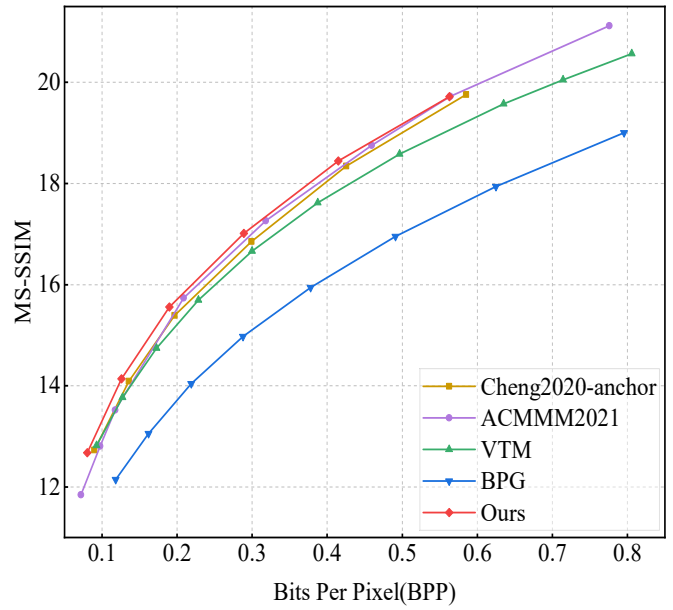
(a) PSNR on Kodak



(b) PSNR on CLIC



(c) MS-SSIM on Kodak



(d) MS-SSIM on CLIC

Fig. 6: Rate-distortion performance curves aggregated over the Kodak and CLIC. MS-SSIM values converted to decibels ($-10\log_{10}(1 - \text{MS-SSIM})$). (a)/(b) and (c)/(d) are results on Kodak and CLIC about PSNR and MS-SSIM, respectively. It indicates our proposed framework is also effective for compressing generic natural images.

